Preprint
UCRL-JC-144009-REV-1

Cookoff Response of PBXN-109: Material Characterization and ALE3D Thermal Predictions

M. A. McClelland, T. D. Tran, B. J. Cunningham, R. K. Weese, and J. L. Maienschein

This article was submitted to 2001 Insensitive Munitions & Energetic Materials Technology Symposium, Saint-Malo, France, June 23 – 27, 2003

U.S. Department of Energy
Lawrence Livermore National Laboratory

August 21, 2001

Cookoff Response of PBXN-109: Material Characterization and ALE3D Thermal Predictions*

M. A. McClelland, T. D. Tran, B. J. Cunningham, R. K. Weese, and J. L. Maienschein

ABSTRACT

Materials properties measurements are made for the RDX-based explosive, PBXN-109, and initial ALE3D model predictions are given for the cookoff temperature in a U.S. Navy test. This work is part of an effort in the U.S. Navy and Department of Energy (DOE) laboratories to understand the thermal explosion behavior of this material. Benchmark cookoff experiments are being performed by the U.S. Navy to validate DOE materials models and computer codes. The ALE3D computer code can model the coupled thermal, mechanical, and chemical behavior of heating, ignition, and explosion in cookoff tests. In our application, a standard three-step step model is selected for the chemical kinetics. The strength behavior of the solid constituents is represented by a Steinberg-Guinan model while polynomial and gamma-law expressions are used for the Equation Of State (EOS) for the solid and gas species, respectively. Materials characterization measurements are given for thermal expansion, heat capacity, shear modulus, bulk modulus, and One-Dimensional-Time-to-Explosion (ODTX). These measurements and those of the other project participants are used to determine parameters in the ALE3D chemical, mechanical, and thermal models. Time-dependent, two-dimensional results are given for the temperature and material expansion. The results show predicted cookoff temperatures slightly higher than the measured values.

INTRODUCTION

Computational tools are being developed to predict the response of Navy ordnance to abnormal thermal (cookoff) events. The Naval Air Warfare Center[1] (NAWC) and Naval Surface Warfare Center (NSWC) are performing cookoff experiments to help validate DOE computer codes and associated thermal, chemical, and mechanical models. Initial work at the NAWC is focused on the cookoff of an aluminized, RDX-based explosive, PBXN-109 that is initially confined in a tube with sealed ends (see Figure 1). The tube is slowly heated until ignition occurs. The response is characterized using thermocouples, strain gauges, and high-speed cameras. A modified version of this system is being developed at the NSWC. The designs of these cookoff systems are relatively simple to facilitate initial model development. An effort is being made to achieve a wide range of results for reaction violence.

Lawrence Livermore National Laboratories (LLNL) and Sandia National Laboratories (SNL) are developing computer codes and materials models to simulate cookoff for ordnance safety evaluations. The computer program ALE3D from LLNL is being used to simulate the coupled thermal transport, chemical reactions, and mechanical response during heating and explosion[2]. SNL is employing multiple computer codes in a parallel effort[3,4,5]. For the analysis of PBXN-109 cookoff, Schmitt et al.[6] performed an initial survey of measured materials properties and provided estimates for several others. In addition, they performed initial predictions of the time to explosion for a small-scale NSWC cookoff system. Erikson et al. [7] performed thermal, chemical, and mechanical simulations of the NAWC tests. Their predicted cookoff temperatures are generally in close agreement to values measured in several NAWC tests. They also present initial calcuations showing the expansion of the containment tube after ignition. In an earlier paper[8], we discussed ALE3D models for cookoff of PBXN-109 in the NAWC system of Figure 1, and presented measurements for thermal expansion, heat capacity, shear modulus, bulk modulus, and ODTX. Here we use those measurements to determine model parameters, and present initial thermal, mechanical, and chemical results for cookoff up to the point of ignition.

---

* Approved for public release, distribution is unlimited.

This work was performed under the auspices of the U.S. Department of Energy by the University of California, Lawrence Livermore National Laboratory under Contract No. W-7405-Eng-48.

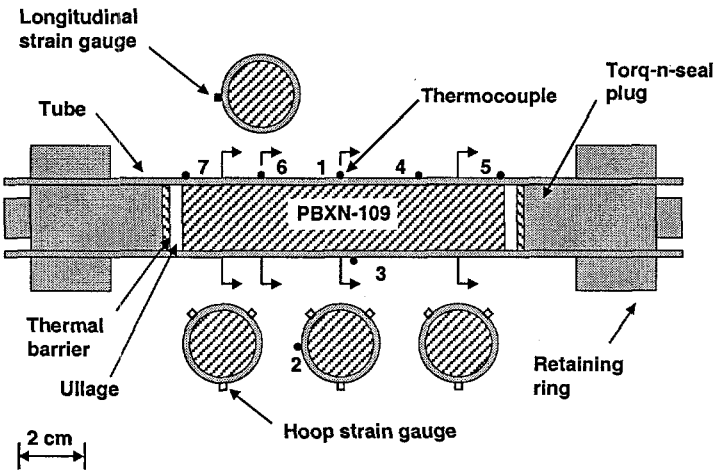

Figure 1 Schematic of geometry and instrumentation for NAWC cookoff in Test No. 000407.

MODEL VALIDATION EXPERIMENTS

The NAWC is performing cookoff tests with cylindrical charges of PBXN-109 confined in a steel tube with sealed ends[1] (see Figure 1). The explosive has a nominal aspect ratio of L/D=4, and a diameter nearly matching the inside diameter of the tube. For a representative test (No. 000407) the 4130 steel tube has a 2.54 cm outer diameter with a 0.89 mm wall thickness providing a confinement pressure of approximately 0.3 kbar (30 MPa). The end seals are achieved with torque-n-seal plugs secured with retaining rings. Ullage is adjusted at the ends of the energetic material by changing the axial positions of the end plugs. Insulating materials are placed at the ends of the explosive and tube. An insulated wire wrap provides the energy to heat the tube. The assembly is mounted horizontally in a vise and enclosed in a sealed box.

For Test No. 000407, the temperature is measured at seven locations on the outer tube surface using thermocouples. A Proportional-Integral-Derivative controller is used to adjust the heater power to keep the center-top temperature, TC1, near the set-point value. Nine hoop strain gauges and one longitudinal strain gauge are used to measure the deformation of the tube during thermal ramp and explosion. A high-speed camera is available to monitor the expansion and fragmentation of the assembly. In this experiment, the final ramp rate for the set-point temperature was 6°C/h.

ALE3D MODEL

ALE3D chemical, mechanical, and thermal models are being developed to model the cookoff of PBXN-109. In our initial model, the chemical reaction sequence is taken to have four components with three reaction steps following the model developed by McGuire and Tarver[9] for pure RDX:

$$A \rightarrow B \qquad r_1 = Z_1 \exp(-E_1/RT)\rho_A \qquad (1)$$

$$B \rightarrow C \qquad r_2 = Z_2 \exp(-E_2/RT)\rho_B \qquad (2)$$

$$C \rightarrow D \qquad r_3 = Z_3 \exp(-E_3/RT)\rho_C^2 \qquad (3)$$

Here ρ_i is the mass concentration of a reactant i. The quantities r_j, Z_j and E_j are the reaction rate, frequency factor and activation energy, respectively, for a reaction j. Component A is the starting material including RDX, aluminum, and binder. Component B is also an intermediate with material properties assumed to be the same as component A, and the components C and D are treated as gases. The aluminum particles and binder are treated as inert until the last reaction step where they are converted to their final products. The selection of parameters and a comparison of model ODTX predictions with measured values is given below.

The mechanical models for the chemical constituents A and B along with the steel components are taken to have Steinberg-Guinan[10] strength models. For PBXN-109, the model expressions for shear modulus and yield stress are taken to be

$$G = G_0 - b(T - T_0) \qquad Y = Y_0 G / G_0 \qquad (4)$$

In which the subscript "0" denotes values at room temperature (20°C). The parameters G_0 and b are estimated from oscillatory shear modulus measurements as described below. A polynomial expression is used for the equations of state:

$$p = p_0 + K_0\mu + a_1\mu^2 + a_2\mu^3 + (\gamma_0+\gamma_1\mu)\rho_0 c_v(T-T_0) \qquad (5)$$

in which

$$\mu = \rho/\rho_0 - 1 \qquad (6)$$

Note that additional terms for strain hardening appear in Eq. (4) for steel[10]. The constant volume heat capacity c_v does not vary with temperature. Calculated melt and cold curves are used to account for the influence of compression on melting energy. In this study, a nonlinear regression procedure is used to determine the coefficients K_0, a, and γ_0 that give an optimum representation of the measurements of CTE, hydrostatic compression, and the unreacted shock Hugoniot described below (see Table 1). The below comparisons between model and experimental values show that the Steinberg-Guinan models provide only an approximate description. The Steinberg-Guinan models were developed for metals, and PBXN-109 is a complex composite material consisting of relatively brittle RDX, rubber-like binder, and loosely-bound aluminum particles. In addition, the Steinberg-Guinan model for 4340 steel is used for the 4130 steel. The influence of these approximations is a subject of continuing investigation.

Table 1 Selected Parameters for Strength and EOS Models

Material parameter	Units	PBXN-109 Solid Species A, B	PBXN-109 Gas Species C, D	4130 steel[10]
K_0	GPa	2.82		159
a_1	GPa	17.3		160
a_2	GPa	144.0		0
γ_0		0.461		1.65
γ_1		0.461		0.5
G_0	GPa	4.68×10^{-3}		77.0
b	GPa/°C	1.10×10^{-5}		5.05×10^{-2}
Y_0	GPa	0.06		1.03
ρ_0	g/cm^3	1.67		7.83
c_v	J/g-°C	1.33	1.96	0.444
λ	W/m-°C			
20°C, 1 bar				42.7
90°C, 1 bar		0.454		
400°C, 1 kbar			7.89×10^{-2}	
2000°C, 1 kbar			7.28×10^{-2}	
Γ			1.163	

The model chemical components C and D are treated as no-strength materials with gamma-law equations of state:

$$p = (\Gamma-1)\,\rho c_v T \qquad (7)$$

This equation of state is appropriate for the relatively low confinement pressures (~1 kbar) of these cookoff tests. The Γ-value for species C and D is set using a pressure of 1 kbar, a temperature of 2273°K, and the density and heat capacity c_v from the thermo-chemical equilibrium computer code, CHEETAH 2.0[11] for the final product gases (see Table 1).

The time-dependent thermal transport model includes the effects of conduction, reaction, advection, and compression. The constant-volume heat capacity is constant for each reactant consistent with the Steinberg-Guinan model. The thermal conductivity for the solid species A and B is taken to be constant, whereas the effects of temperature are included for the gaseous species. The thermal properties for materials A and B are listed in Table 1 and are assigned using the measurements of this project for PBXN-109 as describe below. The heat capacity c_v for gases C and D is assigned the same constant-volume value used in the gamma-law model. The temperature-dependent thermal conductivity is estimated at 1 kbar using Bridgman's[12] equation for liquids in which the sound velocity is calculated using results from CHEETAH (see Table 1).

MATERIALS MEASUREMENTS AND MODEL REPRESENTATION

Here we report on our measurements and ALE3D model representations of shear modulus, bulk modulus, Coefficient of Thermal Expansion (CTE), heat capacity, and one-dimensional-time to explosion for PBXN-109. Also discussed are the calculation of model parameters from shock Hugoniot and thermal conductivity measurements. The PBXN-109 mixture has a nominal composition of 64% RDX, 20% Al, and 16% HTPB/DOA binder by weight[13] . The samples were taken from mixture no. 991206 that is being used by the participants from LLNL, SNL, NAWC, and NSWC in this cookoff investigation. The density for this sample was measured by Paiz and Carey[14] to be 1.67 g/cm^3.

Shear Modulus

The shear storage and loss moduli were measured for PBXN-109 as a function of strain rate and temperature using a Rheometrics Mechanical Spectrometer. Rectangular samples 3.18 x 1.27 x 0.318 cm were cut for testing. Three room temperature tests were performed at a frequency of 1 cycle/s. In each test, the strain was increased from 0 to 1.8%, which increased the shear rate from 0 to 0.11 s^{-1} (see Figure 2). The average shear storage modulus decreases approximately 26% as the shear strain and rate increases (see Figure 2). The standard deviation for the storage modulus is approximately 13% for the three runs. The loss modulus is approximately a factor of five less than the storage modulus. Measurements for the shear storage and loss moduli were made at 1 cycle/s over the temperature range 25 to 120°C. The storage and loss moduli decrease by approximately 25 and 75%, respectively, as the temperature is increased (see Figure 3). The primary contributions to measurement error are irregularities in the sample geometry and alignment of the sample in the test fixtures.

The shear storage modulus measured versus temperature at 1 cycle/s is used as an approximation for the shear modulus in the Steinberg-Guinan model (see Figure 3). A linear fit expression provides a good representation of the measurements, and the fit parameters are listed in Table 1 as G_0, and b for values at T_0=20°C (see Eq. (4)). The yield stress Y_0 is determined from shear strength measurements in other oscillatory shear experiments[15] at 1 Hz.

Bulk Modulus

The bulk modulus was measured by means of a confined compression test[16,17]. The hydraulic piston of a Materials Testing System (MTS) machine was used to uniaxially compress a 1.27 cm D x 2.54 cm L sample in a cylindrical die of the same diameter. In each test, the displacement of the piston was measured while the load was increased at a constant rate. Corrections were made in the displacement data for deflection of the test fixtures. This method was selected since it can provide good results for rubber-like materials in which the shear modulus is small compared to the elastic modulus[16,17] (Poisson's ratio~0.5). In this situation, the compressive loading is nearly hydrostatic.

In order to verify the method, bulk modulus measurements were made for Silastic J, a well-characterized rubber. At room temperature, the compressive stress was increased from 0 to 31.0 MPa at a rate of 0.690 MPa/s. The measured compressive stress for Silastic J is plotted versus volumetric strain in Figure 4. These results compare quite favorably to the measurements of DeTeresa[18]. The latter

measurements were obtained by compressing an immersed sample to provide true hydrostatic compression. Strain-dependent expressions for the bulk modulus are obtained for the two sets of results using

$$K = d\sigma/d\varepsilon_v \tag{8}$$

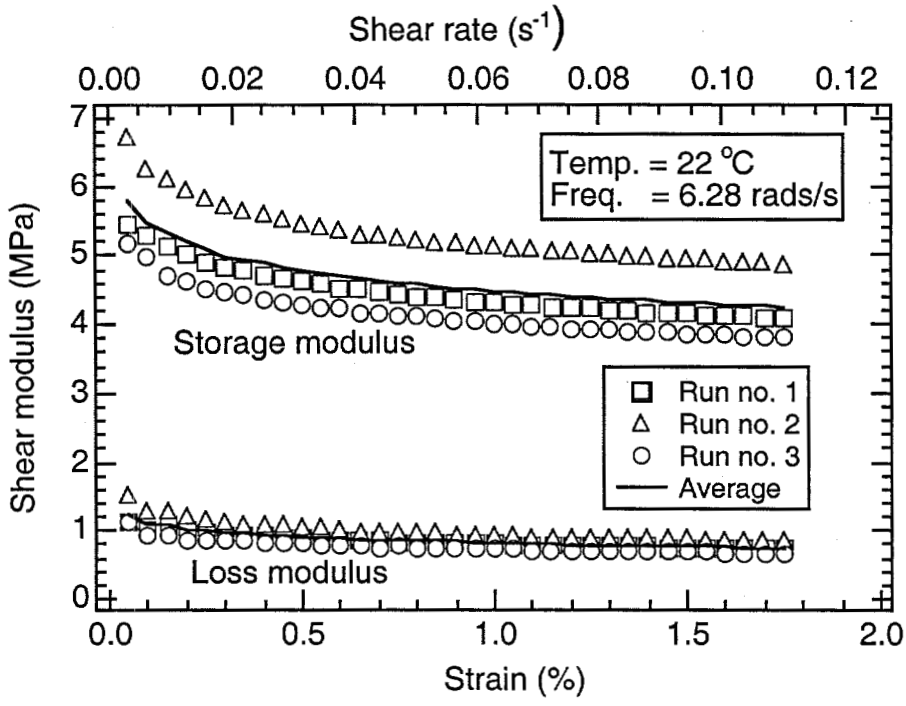

Figure 2 Measured shear modulus versus strain at for PBXN-109 at 1 cycle/s and room temperature.

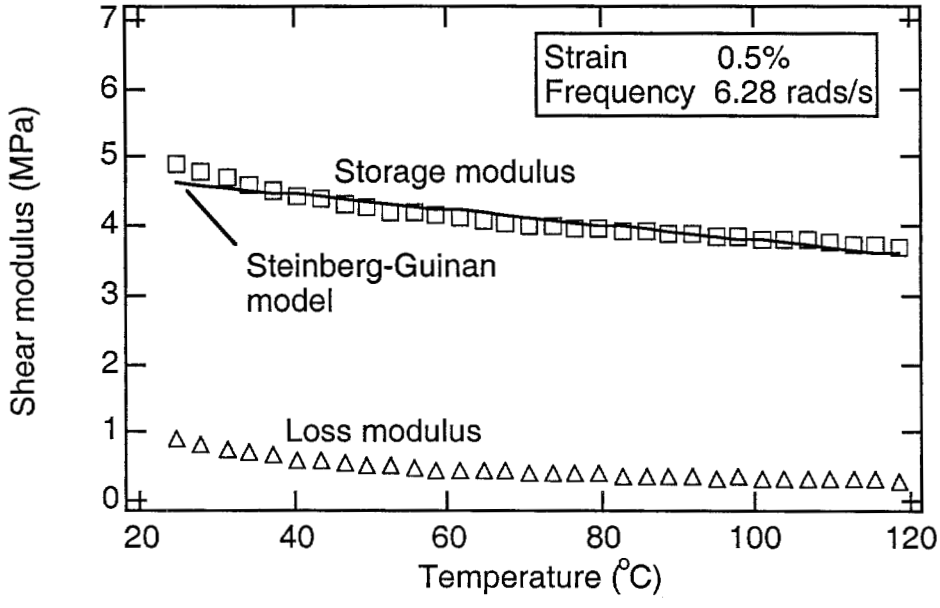

Figure 3 Measured and model shear moduli versus temperature for PBXN-109 at 1 cycle/s and 0.5% strain.

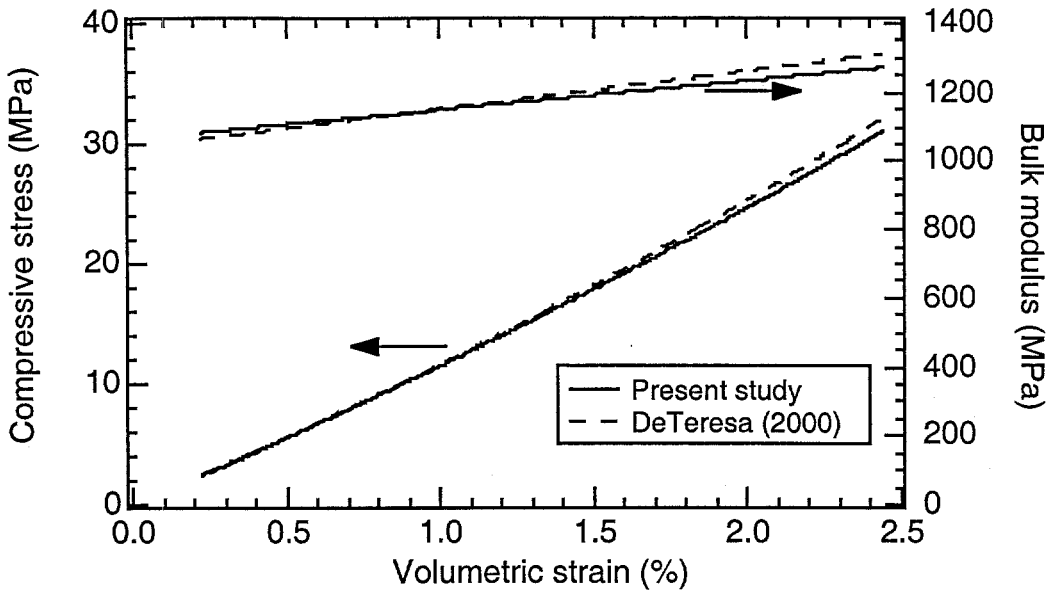

Figure 4 Measured compressive stress and bulk modulus versus volumetric strain for Silastic J at T=22°C.

Here K is the bulk modulus, σ is the compressive stress, and ε_v is the volumetric strain. The resulting curves show a 20% increase in bulk modulus for Silastic J. In addition, there is excellent agreement between the present results and those of DeTeresa[18] (see Figure 4), verifying the correct operation of the apparatus.

Bulk modulus measurements were performed for a single sample of PBXN-109 at room temperature and loads ramped to 69.0 MPa. Three tests were performed for ramp rates of 0.0690, 0.690, and 6.90 MPa/ s (see Figure 5). These were the respective fourth, fifth, and sixth tests with this sample. In the three earlier tests, the sample was loaded to the same stress of 69.0 MPa at a temperature of 22°C. The stress-strain curves are quite similar suggesting that ramp rate has little effect over the range of conditions considered. In addition, it does not appear that repeated mechanical cycling of this sample altered the mechanical properties of the sample in these last three tests. However, there is still the possibility that changes to the sample could have occurred in the first three tests. A fitting procedure was performed to obtain a single composite stress-strain representing all three experimental curves. Application of Eq. (8) to this result gives the bulk modulus curve in Figure 5. It is seen that the bulk modulus varies by a factor of four over the range of strains, indicating that PBXN-109 provides relatively little resistance to compression at low strains, but much more resistance at high strains.

There are several possible sources of experimental error for these measurements. The low modulus at low strains makes it difficult to determine the point of initial compression. In addition, irregularities in the sample geometry lead to uncertainties in the point at which the sample completely fills the die. Both of these factors contribute to an offset uncertainty in the volumetric strain. Finally, it is possible that the repeated load cycling could have altered the mechanical properties from those of the virgin material.

Equation of state values for the pressure are also shown in Figure 5. These values were calculated using the polynomial expression (5) with parameters listed in Table 1. The parameters K_0, a_1, a_2, and γ_0 with $\gamma_1=\gamma_0$ were adjusted using a nonlinear regression procedure to provide a best fit of the CTE, temperature-dependent hydrostatic compression, and the unreacted shock Hugoniot. It is seen that the model provides only an approximate representation of the data. The curvature of the measurements is much greater than the model curve. A more sophisticated model is needed to completely represent the complex behavior of this composite material.

A second set of compression measurements was obtained with the same sample of PBXN-109 at 0.690 MPa/s and temperatures of 20, 50, 75, and 100°C. Measured and model volumetric strains are plotted versus temperature at a compressive load of 68.9 MPa. The volumetric strain is referenced to zero at 20°C and no applied load. At each temperature, the initial measured volumetric strain at no load

is calculated using the CTE of 113 μm/m-°C discussed below. The model curve is calculated using the polynomial EOS (5) with the values listed in Table 1. It provides a good representation of the measured values.

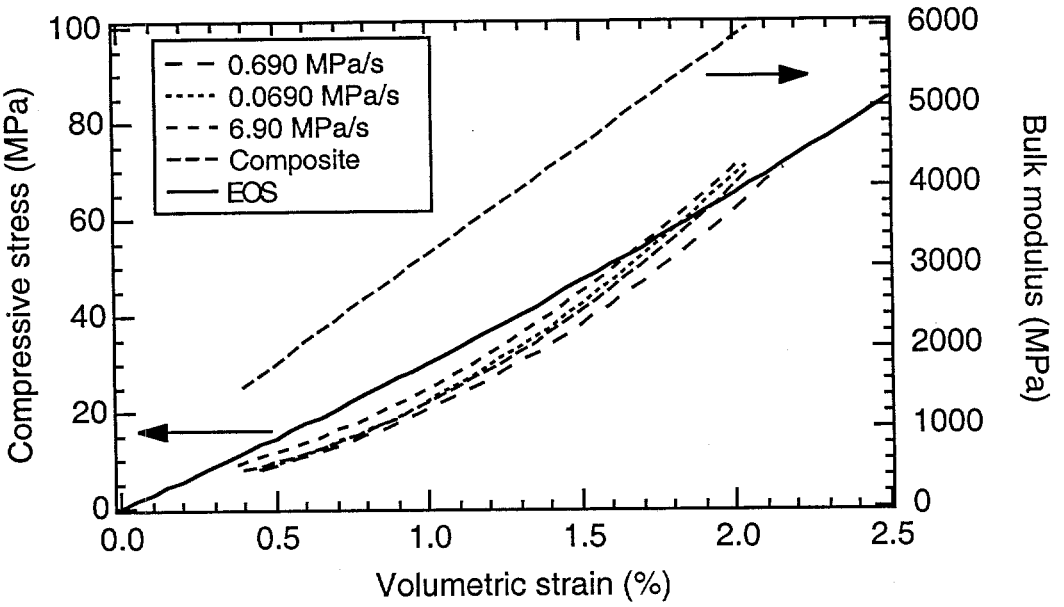

Figure 5 Measured and model compressive stress and bulk modulus versus volumetric strain for PBXN-109 at T=22°C.

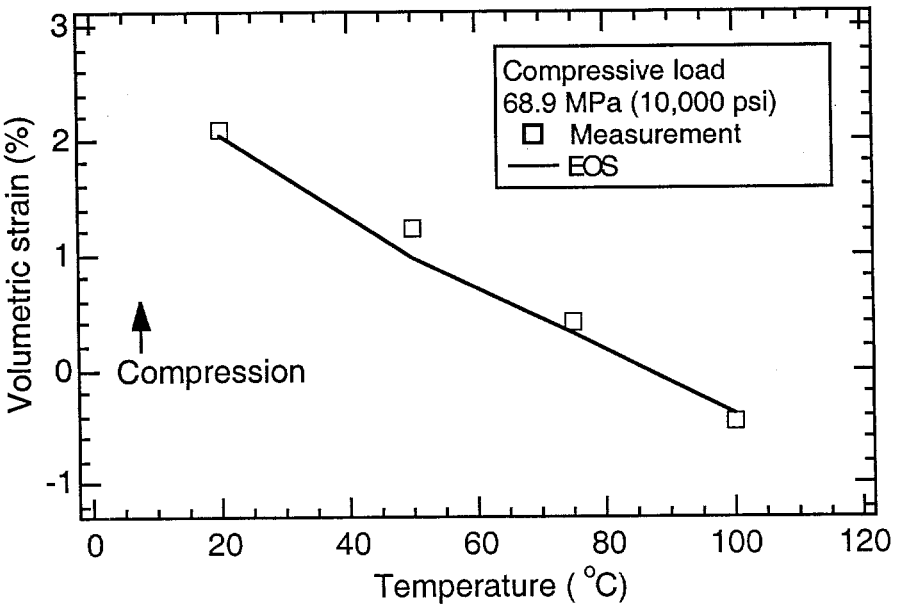

Figure 6 Measured and model volumetric strains versus temperature at 68.9 MPa (10,000 psi).

Estimates for Elastic Modulus and Poisson's Ratio

Rough estimates for Poisson's ratio, ν and the elastic modulus, E, can be obtained using the following expressions with the observation that the measured bulk modulus is two to three orders of magnitude larger than the shear modulus[19], G (see Figures 2 and 5):

$$\nu = (3K - 2G)/(6K + 2G) \approx 0.5 \qquad (9)$$

$$E = 2G(1 + \nu)$$
$$\approx 3G \qquad (10)$$

Here G is taken to be the storage modulus of Figure 2, and the results of Figure 5 are used for K. The rubber-like character of the material is confirmed with the estimated value of 0.5 for Poisson's ratio. This result validates a key assumption of the test that the shear modulus is much less than the bulk modulus.

Unreacted Hugoniot Data

Measurements for the unreacted shock Hugoniot for the PBXN-109 constituents are used to estimate the compression of PBXN-109 at high pressures. Data for RDX[20], alumunium[10], and HTPB binder[21] are combined using the mixing rule of Reaugh and Lee[21] in which the component volumes are added at a given pressure. The constituent and PBXN-109 mixing-rule results are plotted as pressure versus volumetric compression $\mu = \rho/\rho_0 - 1$. They are compared with the values calculated from the polynomial Eq. (5) in Figure 7. It is seen that although there are considerable variations in compliance between materials, the PBXN-109 mixing-rule results are similar to those for RDX. It is also evident that the model representation of the PBXN-109 mixing-rule results is only approximate.

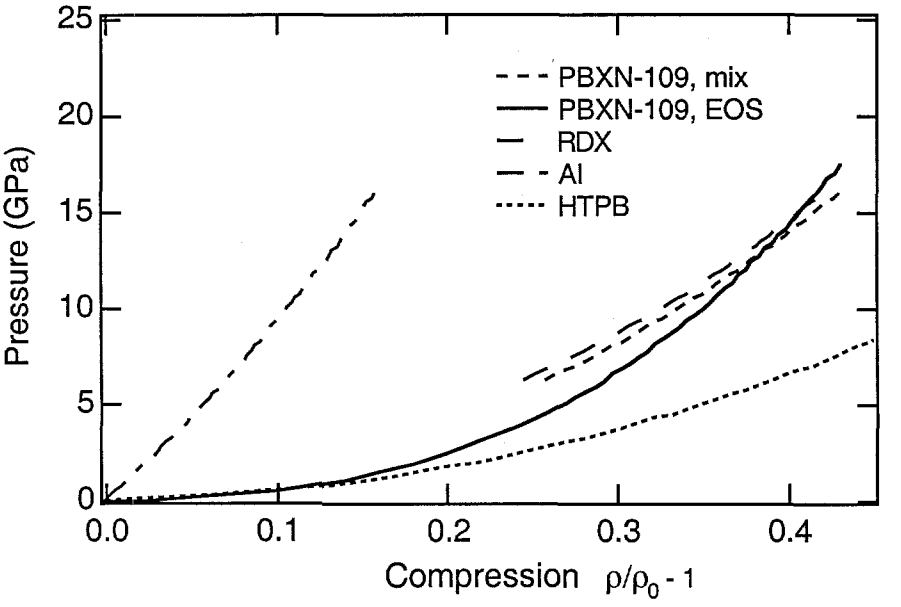

Figure 7 Comparison of model, constituent, and mixing rule Hugoniot curves for pressure versus compression.

Coefficient of Thermal Expansion

Measurements of linear CTE were made for PBXN-109 using a Thermal Mechanical Analyzer (TMA) Model No. 2940 from TA Instruments. Calibration of the instrument was verified with an aluminum standard over the temperature range 25-114°C. The measured aluminum value of 24.6 μm/m-°C agrees well with the standard value of 24.8 μm/m-°C. Measurements for PBXN-109 were made on 0.635 cm D x 0.635 cm L cylinders cut from larger samples. Variations in the sample dimensions and mounting were larger for this material than for a typical metal or explosive due to the rubber-like character of this material. Three tests for PBXN-109 yielded a CTE of 113±8 μm/m-°C for a nominal temperature range of 25 to 115°C (see Figure 8). Although the CTE is nearly constant over this range of temperatures, the small curvature may be lead to errors for large extrapolation. The primary contribution to measurement variation is believed to be the uncertainties in sample dimensions and alignment of the sample in the test fixtures. The measured CTE for PBXN-109 is in the general range of 100-200 μm/m-°C for polymeric materials, and is considerably higher than the values of 25 and 64 μm/m-°C for Al and RDX[22],

respectively. The polynomial equation (5) used to model the CTE, hydrostatic compression, and the unreacted shock Hugoniot data provides a good representation of the thermal expansion data.

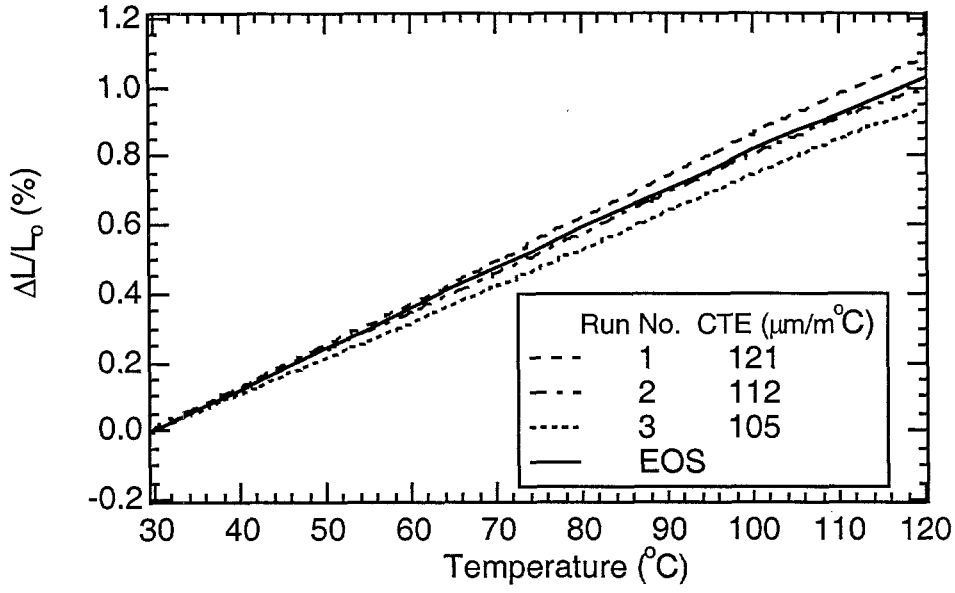

Figure 8 Measured thermal expansion of PBXN-109.

Heat Capacity and Thermal Conductivity

The heat capacity at constant pressure for PBXN-109 was made using a Differential Scanning Calorimeter (DSC) Model No. 2920 from TA Instruments[23]. The DSC measures the difference in the heat flow between a sample and an inert reference as the temperature of the stage is changed. The instrument was calibrated using a sapphire (Al_2O_3) standard and verified using a polystyrene (PS) standard. The 0.343 cm D x 0.0635 cm H sapphire standard was selected for the calibration since it could be used at the highest temperature of 140°C for PBXN-109. In contrast, temperatures for the 0.474 cm D x 0.085 cm H polystyrene sample are kept below 80°C to avoid thermal alteration. The small thickness of each sample provides rapid thermal transport which minimizes thermal lag in the heating of the sample. All samples were encapsulated in aluminum pans, and a relatively high temperature ramp rate of 10°C/min was selected for operation. Baselines were established using empty pans that were crimped together in the manner of the sample pans. Replicate measurements were performed for each standard. Measured values of the PS heat capacity agree with each other to within 1% for a given encapsulated sample. The averages of these measurements are within 1% of the standard values[24] (see Figure 9). The primary contributions to measurement error are believed to be variations in thermal contact resistance between the encapsulating aluminum pans, stage, and sample. Variations in encapsulation and crimping of the sample and reference pans have been observed to contribute several percent variations to the heat capacity results. This variation is much larger than the above-mentioned deviations of 1% associated with run-to-run variations with a single encapsulated sample. In addition, the lower thermal diffusivity for PS increases the thermal lag relative to sapphire. Finally, the rapid ramp rate amplifies these effects.

A 0.5 cm D x 0.1 cm H disk of PBXN-109 was fabricated and encapsulated in aluminum pans for heat capacity measurements. Measurements were made in two runs for this sample over the temperature range of 40-140°C (see Figure 9). The results from the replicated runs agree with each other to within 1% and the averaged values agree with the curve-fit results from Hanson-Parr[25] to within 3%. For the Hanson-Parr data, the sample standard deviation is approximately 9%. At a given temperature, typically 6 measurements were made to give a standard deviation of the mean $\sigma/n^{1/2}$=4%. Thus, the measurements of the two studies agree within measurement uncertainty. In addition to the factors mentioned above, irregularities in the sample shape from cutting may have added to thermal contact resistance and measurement error.

A representative heat capacity at constant volume, c_v, is calculated for use with the polynomial equation of state for solid species A and B at a temperature of 90°C. The standard thermodynamic expression[26]

$$c_p - c_v = T\beta^2/\kappa\rho \qquad (11)$$

is used in which $\beta=(\partial\ln(1/\rho)/\partial T)_p$ and $\kappa=-(\partial\ln(1/\rho)/\partial p)_T$ are the expansivity and compressibility coefficients, respectively. The measured values of CTE, bulk modulus at $\mu=0$, and c_p of this study are inserted into Eq. (11) to give the value for c_v in Table 1.

The thermal conductivity of solid PBXN-109 is calculated using the curve fit for c_p of this study, the measured thermal diffusivity of Hanson-Parr[24], and the density adjusted for the thermal expansion of this study. Specifically, we use $c_p=1.086+3.223\times10^{-3}T$ and $\alpha=3.366\times10^{-3} - 2.183\times10^{-5}T + 7.144\times10^{-8}T^2$ in which α, c_p, λ, and T have the units of cm^2/s, J/g-°C, W/cm-°C, and °C, respectively. The result at 90°C is listed in Table 1.

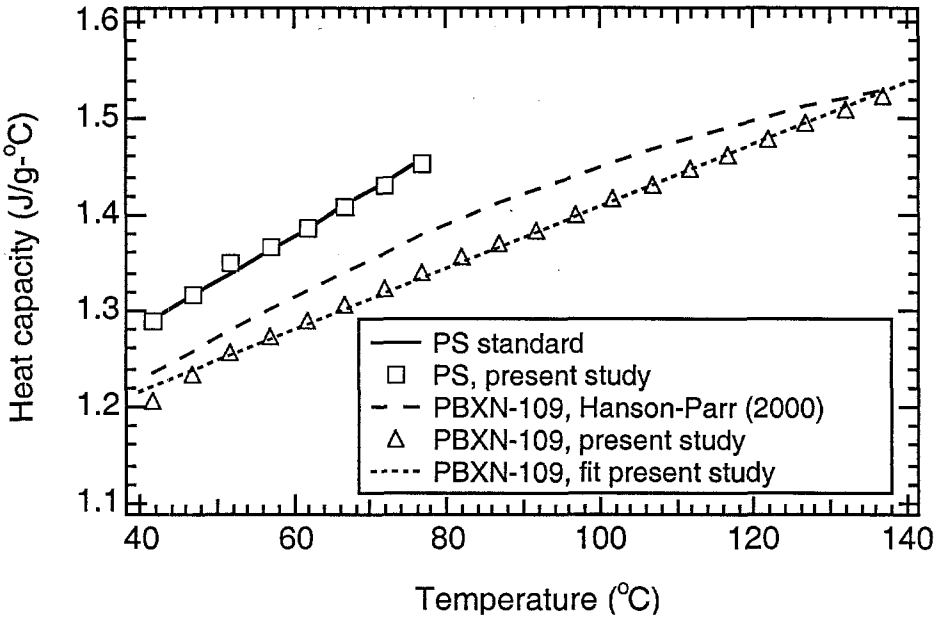

Figure 9 Comparsion of heat capacity measurements for polystyrene and PBXN-109.

One-Dimensional-Time-to-Explosion (ODTX)

ODTX measurements were made using the standard apparatus at LLNL[27]. The central components of the ODTX apparatus are two identical cylindrical aluminum anvils, each containing a hemispherical sample cavity with a diameter of 1.27 cm and a knife-edge groove to accommodate a Cu gasket. A circular copper ring with 1.85 cm diameter is used to establish a gas-tight seal when the two anvils are pressed together. This provides an effective confinement area of 2.7 cm^2. The closing force is established by the hydraulic cylinder (effective area is 20.3 cm^2) pushing on the top anvil. The anvil confinement pressure can be set at 150 MPa by using a hydraulic pressure of 20 MPa (3000 psi). For unconfined tests, a 1 mm square groove was machined in one of the anvil surfaces providing a small opening when the anvils were pressed together. Preferential discharge of smoke from this opening indicated that the sample cavity was sufficiently exposed to ambient conditions.

PBXN-109 samples were hand carved into 1.27 cm diameter spheres. A 1.59 cm diameter cylinder is first cored from the bulk sample using a brass coring tool. Cylindrical pieces slightly longer than 1.27 cm length were then sectioned out using a razor blade. Finally, a 1.27 cm-diameter scoop (similar to a mellon baller) was used to round off the pieces to produce the final spheres. The surface was also smoothed using the same tool. Sample weights are reproduced to within 10%.

In these experiments, the anvils were preheated to a pre-determined temperature. The anvils were briefly opened to allow delivery of a spherical explosive sample into the cavity. The anvils were then closed, and confinement was established with hydraulic force. When the internal cavity pressure exceeds that of the closing force, the anvils pop apart with a loud report. The time to explosion is the elapsed time between the insertion of the spherical sample and the rupture of containment as registered by the microphone. A series of experiments were conducted with time to explosions ranging from 30 seconds to several hours.

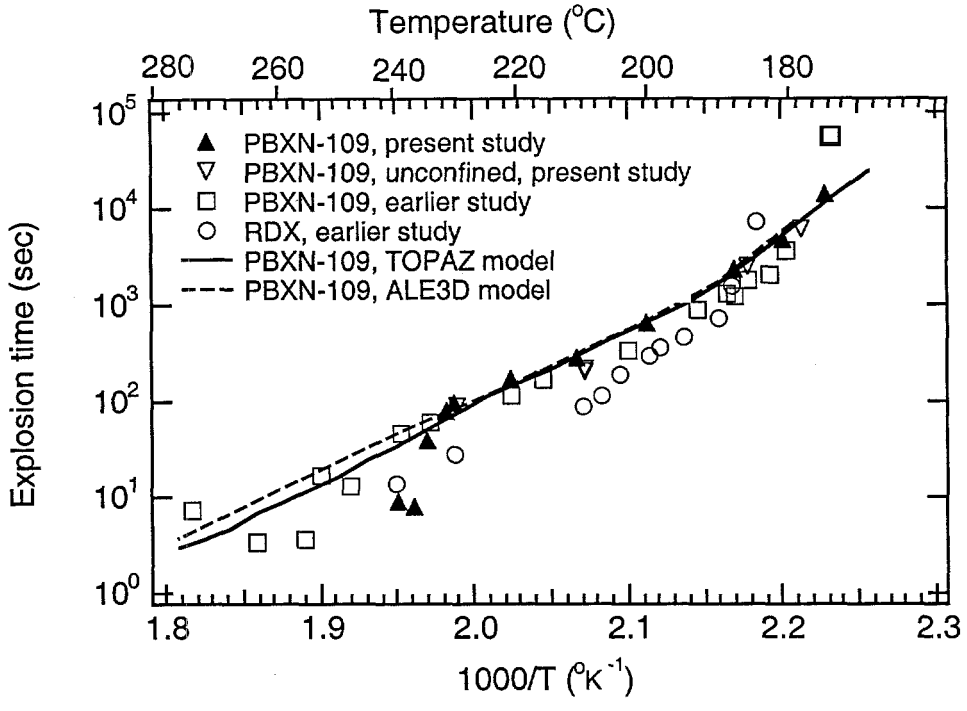

Figure 10 Comparison of ODTX results for PBXN-109 and RDX.

The time to explosion for PBXN-109 as a function of temperature for samples under no confinement and heavy confinement (150 MPa) is shown in Figure 10. Results from earlier ODTX tests with PBXN-109 and RDX at 150 MPa confinement are also included for comparison. The confined and unconfined results of this study follow a single curve, indicating experimental reproducibility and the insensitivity of explosion time to pressure. These results are consistent with the earlier PBXN-109 results except at temperatures above 235°C. In this temperature range the explosion times of this study show a much stronger sensitivity to temperature. The scatter in the earlier PBXN-109 data is much larger at the higher temperatures and associated short explosion times of 1 to 10 s, suggesting an approach to the measurement limits of the apparatus. The earlier RDX explosion times are generally shorter than the PBXN-109 values. The thermal diffusivity of 3×10^{-3} cm^2/s for PBXN-109 is considerably higher than the RDX value of 5×10^{-4} cm^2/s which would tend to reduce hot spots in the PBXN-109 and make it less reactive relative to RDX. At lower temperatures and longer explosion times, the importance of thermal transport is reduced and behavior is governed by the reaction kinetics of RDX, leading to similar explosion times for RDX and PBXN-109.

Calculated explosion times for PBXN-109 are also shown in Figure 10 for a one-dimensional model[9] involving transient heat conduction and the chemical reaction sequence (Eqs. (1)-(3)). In this model, the densities of each of the four components A, B, C, and D are taken to have the room temperature value of 1.67 g/cm^3. The two components A and B are assumed to have the same thermal transport properties. We use the heat capacities and thermal conductivities of Table 1. The values of E_j in Table 2 are the same as those of McGuire and Tarver[7]. The values of $\ln(Z_j)$ are shifted by a single offset value as described below to provide an optimal fit of the confined measured explosion times. A model to

satisfactorily represent all of the measurements has not yet been completed. The two highest temperature points were not included in the regression procedure in order to provide a better fit of the lower temperature data that is most relevant to slow cookoff. The RDX heats of reaction q_1 and q_2 for the first two steps are reduced by 36% to account for the fraction of RDX present in

Table 2 Chemical Kinetics Parameters for PBXN-109

Reaction step	$\ln(Z_j)$	E_j kcal/g-mole-°K (kJ/g-mole-°K)	q_j cal/g (J/g)
A→B	43.7 s^{-1}	47.1 (197)	64 (268) endothermic
B→C	38.9 s^{-1}	44.1 (185)	-192 (-803) exothermic
C→D	32.7 s^{-1}-cm^3- g^{-1}	34.1 (143)	-1568 (-6560) exothermic

the mixture. The aluminum and the binder are treated as inert until the final reaction step. The value for q_3 is calculated using q_1 and q_2 and the total heat of reaction of 1696 cal/g calculated from CHEETAH. One-dimensional explosion times were calculated using TOPAZ2D[28,29] and a mesh with 50 elements uniformly spaced in the radial direction. The time to explosion is taken to occur at the time that 10% of the initial mass of HE is converted to the final product D[9]. A nonlinear regression procedure incorporating the Davidon-Fletcher-Powell method[30] was used to adjust the single shift in $\ln(Z_j)$ to provide the best fit of the measured values by the TOPAZ2D values. The resulting model explosion times match the measured values over much of the temperature range (see Figure 10). However, there are larger discrepancies between the model values and the measurements of this study at temperatures above 235°C. It is also of interest to note that in this same temperature range measurements of the current study differ significantly from the results of the earlier study which exhibit considerable scatter. Nonetheless, the model is expected to provide satisfactory results at the lower temperatures observed at ignition in the cookoff tests.

Also shown in Figure 10 are results for the ALE3D code for the case of reaction and thermal transport without material motion. We use the same parameters of Tables 1 and 2 employed with TOPAZ2D. Additional details are given below on the solution strategy. We used a 1D spherically symmetric mesh that also has 50 uniform elements (see Figure 11a). The results agree within 2% for temperatures below 235 °C, but variations of the scale 10% are seen for higher temperatures. This discrepancy is attributed to incomplete resolution of the conduction boundary layer at short times which is less important in slow cookoff cases.

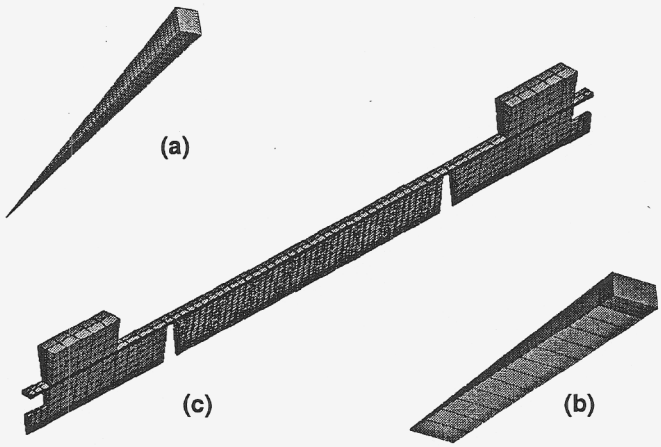

Figure 11 ALE3D meshes: (a) ODTX 1D, 50 zones. (b) Test 000407 1D, 15 zones. (C) Test 000407 2D, 1576 zones.

BOUNDARY CONDITIONS AND NUMERICAL METHOD

Boundary Conditions

One and two-dimensional ALE3D models for PBXN-109 (see Figure 12) are used to simulate the cookoff setup of Test No. 000407 (see Figure 1). The two-dimensional model includes 10% ullage on the HE ends and 0.4% ullage on the side. Surfaces across the gap expand and slide without friction and have negligible thermal contact resistance. The plug and retaining ring are assumed to be perfectly joined to the tube wall. The ends of the tube and plug at the spacer block are treated as free mechanical boundaries in which energy losses are handled with a heat transfer coefficient. The tube heater is modeled as a uniform thermal flux condition at the outside tube surface between the retaining rings. The heat flux is adjusted using a PI controller to maintain TC1, the top-center tube temperature, at its set-point value (see Figures 1, 12). The PI controller is tuned using the strategy of Internal Model Control[31] in which the steel tube wall is treated as a first-order lumped-capacitance system with a single heat transfer coeffcient to account for thermal losses to the surrounding air. Thermal convection is applied to all outward facing surfaces using heat transfer coefficients for laminar flow of air past a horizontal cylinder[32]. Standard expressions for hemispherical radiation are used on these same surfaces. Heat transfer coefficients are reduced on the outside surface of the heater to account for the influence of insulation.

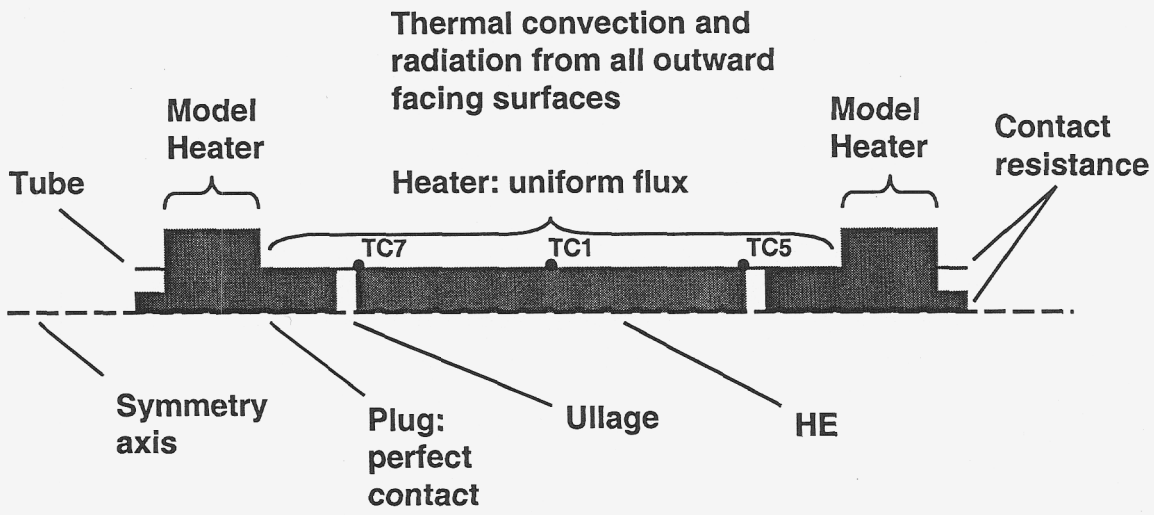

Figure 12 Boundary conditions for ALE3D axisymmetric model of NAWC cookoff Test No. 000407.

Since there are large uncertainties concerning contact resistances between the plug, tube, and vise, adjustments are made in the heat fluxes at the outside surface of the rings. Model PI controllers are added to adjust the uniform heat flux at these surfaces to match linear representations of the measured temperatures at the end thermocouples TC5 and TC7. Each end thermocouple trace is fit by the expression

$$T = T_\infty + c(T_{set} - T_\infty) \qquad (12)$$

in which c is the fit parameter, T_{set} is the set-point temperature for TC1, and T_∞=20°C is the ambient temperature. The resulting two fit expressions are used as set points for two additional model PI controllers. This approach allows the thermal conditions to be accurately represented for evaluation of the HE response.

The domain for the one-dimensional model is the symmetry plane between the axial ends of the tube. The small ullage of 0.4% is treated as negligible. The wall temperature is controlled with the same PI controller as for the 2D case, and the same models are used for thermal losses from the tube wall.

Meshes and Numerical Strategy

The ALE3D computer code requires 3D meshes, and wedge-shaped meshes are employed for the 2D and 1D models of this study (see Figure 11). A small hole is present near the symmetry axis to allow the use of hexahedral elements at all locations. The zones in both meshes are concentrated in the HE, and the same radial resolution (12 zones) is applied in each mesh. The effects of mesh refinement were explored by increasing the number of zones in the radial direction for the 1D mesh by a factor of 8.

For the 1D model without ullage, fully-implicit integration schemes are applied for both material motion and thermal transport. For the 2D model, the integration of the thermal transport equation is performed in the same manner. However, the presence of ullage in the 2D model currently requires an explicit integration method for the momentum equation. In order to provide for practical computation times, the density in the inertial term is increased. This approach is valid in the limit of small material motion, and is applicable to the long thermal ramps of this study.

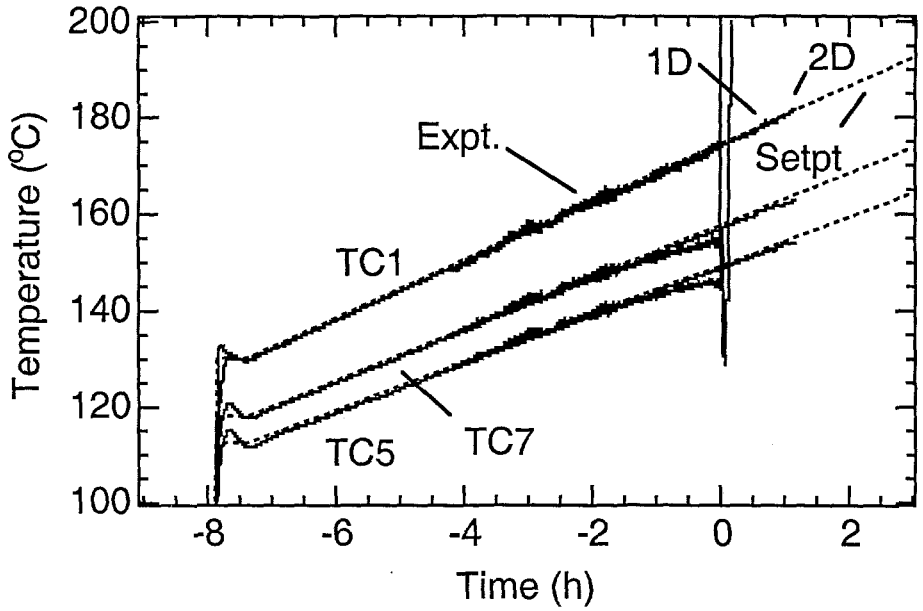

Figure 13 Comparison of temperatures for measurements, set points, and ALE3D 1D and 2D models.

COMPARISON OF ALE3D AND MEASURED THERMAL COOKOFF RESULTS

In cookoff Test 000407 for PBXN-109, the set-point temperature for TC1 was increased at 600°C/h from room temperature to 130°C, held for 0.5 h, and then increased at 6°C/h until cookoff (see Figures 1 and 13). The measurements begin during the second ramp. The thermocouple, TC1, tracks the set point with some noticeable fluctuations (±1°C) until cookoff at a set-point temperature of 176°C. The top-end thermocouples TC7 and TC5 show temperatures nominally 15 and 25 °C less than the set-point temperature, respectively. This indicates considerable cooling at the tube ends, particularly at the right end. Thus, large temperature gradients are present along the length of the HE, creating a well-defined hot zone near the axial midplane.

The model controller tracks the TC1 set point well through both the fast and slow ramps (see Figure 13). Note that the controller gain was reduced by a factor of four after the initial steep ramp to increase numerical efficiency during periods of slow change in the set point. The TC5 and TC7 traces were fit according to the procedure described above, and used as set-points in the two auxillary model controllers providing heat at the outside surfaces of the retaining ring. Although there is some overshoot for the 2D model at TC5 and TC7 after the steep ramp, these controllers generally keep the model temperatures near the measured values.

The cookoff temperature for the 2D model is 181.0°C which is somewhat larger than the measured value of 176°C. Note that the cookoff temperature is taken to be the value of the set-point temperature for TC1 at the time of cookoff. In order to help determine the source of this difference, the

1D model is used to explore the impact of cooling at the ends which is zero for the 1D case. The resulting cookoff temperature of 178.4°C, suggesting a minimal influence of uncertainties relating to cooling at the tube ends. The 1D model is also used to examine the possible effects of mesh refinement. The number of zones in the radial direction is increased from 12 to 96 with no signficant change (<1%) in the cookoff temperature. This suggests that the 2D results are sufficiently resolved in space for time-to-event calculations. It is believed that the discrepancy has its source in the chemical kinetics model.

Two-dimensional temperature fields are shown in Figure 14 after the initial steep ramp, after the hold, and prior to cookoff. Strong radial temperature and axial temperature gradients are observed after the steep ramp at the beginning of the hold period. At the end of the hold period, the primary variations are in the axial direction as desired. The predicted ignition location is near the axis of symmetry and axial midplane. This result is confirmed by fragments that show failure in the middle of the tube (see Figure 15). The profiles of Figure 14 also show the expansion of the HE into the steel tube which has a CTE an order of magnitude smaller. The HE expands and fills the small gap at its radial surface early in the steep ramp. Prior to ignition, the HE has expanded to partially fill the gaps at the HE ends.

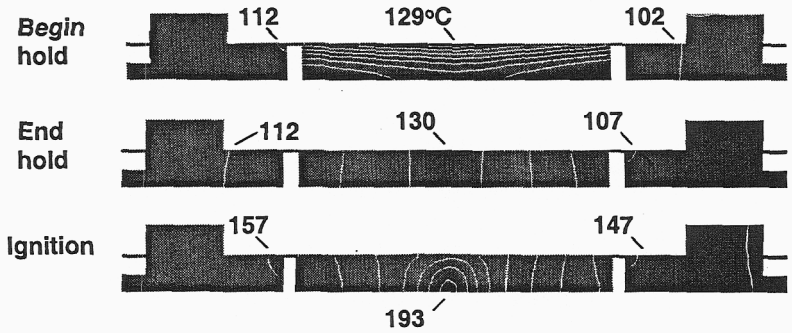

Figure 14 Temperature contours for ALE3D axisymmetric model of NAWC cookoff Test No. 000407. Contours increase from 102°C in 5°C increments.

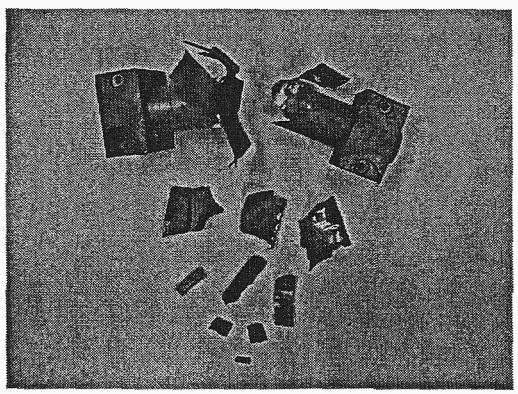

Figure 15 Collected tube fragments for Test No. 000407.

CONCLUSIONS

ALE3D chemical, mechanical, and thermal models are being developed to simulate the cookoff of PBXN-109 in NAWC and NSWC cookoff tests. In the NAWC cookoff experiments, a PBXN-109 sample with L/D=4, is heated slowly in a sealed tube until explosion. Thermocouple measurements and collected fragments for a representative test show ignition in the warm central region of the tube. Mild violence is indicated by the large size of the collected fragments. For the development of ALE3D models, a McGuire and Tarver[9] chemical kinetics model for RDX is applied to PBXN-109. Steinberg-Guinan strength models are used for the solid PBXN-109 species. Polynomial and gamma-law equation of state

expressions are employed for the solid and gas species, respectively. These parameters are determined using measurements for thermal expansion, heat capacity, shear modulus, bulk modulus, and one-dimensional time to explosion. The solid strength and EOS models provide an approximate representation of the complex behavior of this composite material. For a selected NAWC test, the ALE3D temperature fields are matched to the measured fields. The predicted cookoff temperatures are slightly higher than the measured values, and the results show the expansion of HE into void areas.

ACKNOWLEDGMENTS

John Reaugh and Craig Tarver are acknowledged for their valuable input on model development. Albert Nichols and Brad Wallin helped with the development and use of the ALE3D computer code. Mark Hoffman assisted with the shear modulus measurements. For the bulk modulus measurements, Steve DeTeresa provided helpful advice, and Scott Groves assisted with the measurements. Rich Simpson prepared PBXN-109 samples for the materials measurements. Alice Atwood, Pat Curran, and Mark Decker of NAWC-China Lake are acknowledged for their efforts in gathering and interpreting the cookoff data. Bill Erikson of SNL helped with model development.

NOMENCLATURE

A, B, C, D	Components in chemical reaction sequence
a_1, a_2	Parameters in polynomial EOS (Eq. 5)
ALE3D	Chemical-mechanical-thermal code using Abitrary Lagrange Euler meshes in 3D
b	Parameter in Eq. (4), $M/(t^2LT)$
CTE	Coefficient of Thermal Expansion, (1/T)
c_p	Heat capacity at constant pressure, (L^2/t^2T)
c_v	Heat capacity at constant volume, (L^2/t^2T)
DOA	DiOctyl Adipate
DOE	Department of Energy
DSC	Differential Scanning Calorimeter
E	Elastic modulus, $M/(t^2L)$
E_j	Energy of activation for reaction j, E/(Tmole)
G	Shear modulus, $M/(t^2L)$
HTPB	Linear Hydroxy-Terminated Polybutadiene
K	Bulk modulus, $M/(t^2L)$
K_0	Bulk modulus in polynomial EOS (Eq. 5), $M/(t^2L)$
n	Reaction order
p_0	Reference pressure, $M/(t^2L)$
NSWC	Naval Surface Warfare Center, Indian Head
ODTX	One-Dimensional Time to Explosion
PBXN-109	Aluminized RDX explosive
RDX	Cyclotrimethylene trinitramine
RMS	Root Mean Square
r_j	Rate of reaction j, $M/(L^3t)$
T	Temperature, T
T_0	Reference temperature, T
TMA	Thermal Mechanical Analyzer
Y	Yield stress, $M/(t^2L)$
Z_j	Frequency factor for reaction j, $L^{3(n-1)}/(M^{(n-1)}\ t)$
α	Thermal diffusivity, L^2/t
γ_0, γ_1	Parameters in polynomial EOS (Eq. 5)
ε_v	Volumetric strain
λ	Thermal conductivity, E/(tLT)
ν	Poisson's ratio
ρ_i	Mass concentration of reactant i, M/L^3
σ	Compressive stress, $M/(t^2L)$

REFERENCES

[1] Atwood, A. I., Curran, P. O., Decker, M. W., and Boggs, T. L., "Experiments for Cookoff Model Validation," JANNAF 37th Combustion and 19th Propulsion Systems Hazards Subcommittee Meetings, Monterey, CA, pp. 205-220, 2000.

[2] Nichols, A. L., III, Couch, R. McCallen, R. C., Otero, I. and Sharp, R., "Modeling Thermally Driven Energetic Responses of High Explosives," in *Proceedings of 11th International Detonation Symposium,* Snowmass, CO, Office of Naval Research August, 1998.

[3] Gartling, D. K., Hogan, R. E. and Glass, M. W., "Coyote – A Finite Element Code for Nonlinear Heat Conduction Problems," Version 3.0, Part I – Theoretical Background: SAND94-1173, Part 2 – User's Manual: SAND94-1179, Sandia National Laboratories, Albuquerque, NM, 1998.

[4] Summers, R. M., Peery, J. S. Wong, W. K. Hertel, W. S., Trucano, T. G., and Chhabildas, L. C. "Recent progress in ALEGRA development and application to ballistic impacts," SAND96-0045C, Sandia National Laboratories, Albuquerque, NM, 1996.

[5] McClaun, J. M., Thompson, S. L., and Elrick, M. G., "CTH: A Three-Dimensional Shock Physics Code," *Int. J. Impact Engng,* Vol. 10 pp. 351-360, 1990.

[6] Schmitt, R. G., Erikson, W. W., Atwood, A. I. and John, H. "Analysis of the NAWC Validation Cookoff Test," JANNAF 36th Combustion and 18th Propulsion Systems Hazards Subcommittee Meetings, Kennedy Space Center, FL, 1999.

[7] Erikson, W. W., R. G. Schmitt, A. I. Atwood, and P. D. Curran, "Coupled Thermal-Chemical-Mechanical Modeling of Validation Cookoff Experiments", JANNAF 37th Combustion and 19th Propulsion Systems Hazards Subcommittee Meetings, Monterey, CA, 2000.

[8] McClelland, M. A., T. D. Tran, B. J. Cunningham, R. K. Weese, and J. L. Maienschein, "Cookoff Response of PBXN-109: Material Characterization and ALE3D Model," JANNAF 37th Combustion and 19th Propulsion Systems Hazards Subcommittee Meetings, Monterey, CA, pp. 191-204, 2000.

[9] McGuire, R. R., and Tarver, C. M., "Chemical Decomposition Models for the Thermal Explosion of Confined HMX, TATB, RDX, and TNT Explosives," *Seventh Symposium (International) on Detonation,* NSWC MP 82-334, pp. 56-64, 1981.

[10] Steinberg, J., "Equation of State and Strength Properties of Selected Materials," Lawrence Livermore National Laboratories, UCRL-MA-106439, 1996.

[11] Fried, L. E., W. M. Howard, P. C. Souers, "Cheetah 2.0 User's Manual," Lawrence Livermore National Laboratories, UCRL-MA-117541 Rev. 5, 1998.

[12] R. B. Bird, W. E. Stewart, and E. N. Lightfoot, *Transport Phenomena*, Wiley, pp. 260-261, 1960.

[13] Hall, T. N. and Holden J. R., *Navy Explosives Handbook, Explosion Effects and Properties-Part III Properties of Explosives and Explosive Compositions*, NSWC MP 88-116 October, 1998.

[14] Paiz, A. and Carey, N., "Specification Test Analysis of PBXN-109, Mix #991206, for Vacuum Thermal Stability, Immersion Density, Electrostatic, ERL Impact Testing and Composition Analysis 47CP10D Log #-99-12-14-06," NAWC-China Lake memo, 2000.

[15] Heindahl, R., NAWC-CL, personal communication, 2000.

[16] Peng, S. H., Shimbori, T., and Naderi A., "Measurement of Elastomers Bulk Modulus by Means of a Confined Compression Test," *Rubber Chemistry and Technology,* Vol. 7 pp. 871-879, 1994.

[17]Gilmour, I., Trainor, A., and Haward, R. N., "The Determination of the Bulk Modulus in a Constrained Solid," *J. Polymer. Sci,* Vol. 12 pp. 1939-1940, 1974.

[18] DeTeresa, S. J., private communication 2000.

[19] Fung, Y. C., *Foundations of Solid Mechanics,* Prentice Hall, New Jersey, 1965.

[20] Dobratz, B. M. and Crawford, P. C., *LLNL Explosives Handbook, Properties of Chemical Explosives and Explosive Simulants,* Lawrence Livermore National Laboratories, UCRL-52997 Change 2, 1985.

[21] Reaugh, J. E., E. L. Lee, "Shock Hugoniot Behavior of Mixed Phases with Widely Varying Shock Impedances," Proceedings of 1997 Topical Conference on Shock Compression of Condensed Matter, July 27-August 1, 1997, Univ. of Massachusettes, Amherst, MA.

[22] Dobratz, B. M. and Crawford, P. C., *LLNL Explosives Handbook, Properties of Chemical Explosives and Explosive Simulants,* Lawrence Livermore National Laboratories, UCRL-52997 Change 2, 1985.

[23] Bershtein, V.A., Egorov, V.M., *Differential Scanning Calorimetry of Polymers*, Ellis Horwood Limited, 1994.

[24] Gaur, V. and Wunderlich, B., *J. Phys. Chem. Ref. Data.* Vol. 11 (2) pp. 313, 1982.

[25] Hanson-Parr, D. "Thermal Properties Measurements of PBXN-109 Mix #991206", memo Naval Air Warfare Center-China Lake, Feb. 15, 2000.

[26] Denbigh, K. G., *Principles of Thermochemical Equilibrium*, Cambridge Univ. Press, pp. 96-97, 1978.

[27] Catalano, E., McGuire, R., Lee, E. L., Wrenn, E, Ornellas, D., and Walton J., "The Thermal Decomposition and Reaction of Confined Explosives", in *the Sixth International Symposium on Detonation Proceedings*, p. 214, Office of Naval Research, ACR-221, Coronado, CA, 1976.

[28] Shapiro, A. B. and Edwards A. L., "TOPAZ2D Heat Transfer Code Users Manual and Thermal Property Data Base," Lawrence Livermore National Laboratory, UCRL-ID-104558, 1990.

[29] Nichols, A. L. and Westerberg K. W., "Modification of a Thermal Transport to Include Chemistry with Thermally Controlled Kinetics," *Numerical Heat Transfer, Part B,* vol. 24, pp. 489-509, 1993.

[30] Avriel, M. *Nonlinear Programming: Analysis and Methods,* McGraw-Hill, pp. 4-1:4-20, 1970.

[31] Morari, M and E. Zafiriou, *Robust Process Control,* Prentice Hall, pp. 116-117, 1989.

[32] Holman, J. P., *Heat Transfer,* McGraw-Hill, pp. 253-254, 1976.